LIGO SCIENTIFIC COLLABORATION
VIRGO COLLABORATION

Document Type	**LIGO-T2000124-v7** **VIR-0319B-20**	2020/06/24

On the measurement of inspiral higher order modes on GW190814 by coherent WaveBurst

G. A. Prodi[1,2], G. Vedovato[3], M. Drago[4,5], V. Gayathri[6], S. Klimenko[6], C. Lazzaro[7,3], A. Miani[1,2], E. Milotti[8], B. O'Brian[6], F. Salemi[9], M. Szczepanczyk[6], and S. Tiwari[10]

[1]*Università di Trento, Dipartimento di Matematica, I-38123 Povo, Trento, Italy*
[2]*INFN, TIFPA, I-38123 Povo, Trento, Italy*
[3]*INFN, Sezione di Padova, I-35131 Padova, Italy*
[4]*Gran Sasso Science Institute, Via F. Crispi 7, I-67100, L'Aquila, Italy*
[5]*INFN, Laboratori Nazionali del Gran Sasso, I-67100 Assergi, Italy*
[6]*University of Florida, Gainesville, FL 32611, USA*
[7]*Università di Padova, Dipartimento di Fisica e Astronomia, I-35131 Padova, Italy*
[8]*Università di Trieste, Dipartimento di Fisica and INFN Sezione di Trieste, Via Valerio, 2, I-34127 Trieste, Italy*
[9]*Università di Trento, Dipartimento di Fisica, I-38123 Povo, Trento, Italy*
[10]*Physik-Institut, University of Zurich, Winterthurerstrasse 190, 8057 Zurich, Switzerland*

Abstract

The detection and waveform reconstruction of gravitational wave transients on LIGO-Virgo data is pursued by a variety of methods, either exploiting detailed signal models or using minimal assumptions on the signal morphology [1]. The coherentWaveBurst (cWB) pipeline [2] provides well established methods both for the detection and for the reconstruction of transient signals. It implements a waveform-agnostic search for a coherent response in the network of detectors in the time-frequency domain by exploiting the Wilson-Daubechies-Meyer (WDM) wavelet transform [3]. Here we present a recently developed analysis procedure based on cWB, targeting the detection of spectral features beyond the quadrupolar emission in the inspiral phase of compact binary coalescences. This method has been used in the GW190814 discovery paper [4] and is an evolution of the methods already described in [5]. The analysis is based on a comparison between the waveform-agnostic reconstruction of the signal provided by cWB and the estimates based on detailed waveform models [6, 7]. The search targets subleading harmonics of the main quadrupolar emission and is performed within suitable slices of the time-frequency representation of the event. These time-frequency slices cover possible chirping-like undertones or overtones in the inspiral phase and their shapes are determined by a mild optimization of the Receiver Operating Characteristic (ROC), see e.g. [8]. The GW190814 results presented in [4] are here

discussed more in depth, providing supplementary material both on the detection of the $m = 3$ mode and on the searches for other subdominant modes, which have been performed over a wide range of possible chirping undertones and overtones.

1 Introductory remarks

CoherentWaveBurst (cWB) provides a well-established set of data analysis methods both for the detection and for the reconstruction of transient gravitational waves [2, 9–11], based on a waveform-agnostic search for a coherent response in the network of gravitational wave detectors [1].

The goal of this technical note is to provide a description of the cWB method to detect possible undertones and overtones of the dominant quadrupolar emission described by the m=2 multipole. This is meant to supplement the related content in the GW190814 discovery paper, [4]. An alternative method is described in reference [12] and its results have been included both in [13] and in the GW190412 discovery paper, [4]. The more general description of the method for comparing cWB reconstructed signals with signal models obtained from Bayesian inference can be found in [5].

The scientific context and latest results on the detection of higher order modes emitted during the inspiral phase of compact binary coalescences are described in [13] and [4].

This note is organized as follows. Section 2 recalls the main steps of the waveform comparison procedure and the definition of the test statistic, i.e. the waveform residual energy. Section 3 describes the choice of the relevant time-frequency portion (slice) where the test statistic is evaluated, in particular the parametrization in terms of harmonics of the dominant quadrupolar emission and the optimization by means of the Receiver Operating Characteristic. Section 4 focuses on the interpretation of the cWB detection of the $m = 3$ subdominant mode and on the multiple searches for possible additional subleading harmonics, discussing detection efficiency and statistical significance from Montecarlo simulations. Section 5 provides our final remarks.

2 Waveform comparison procedure

In [5] we discussed some comparison procedures between the waveform-agnostic reconstruction of the signal provided by cWB and the signal models provided by Bayesian inference methods which exploit detailed waveform models. In this Section we will summarize the main points of that general approach which are relevant for the search for inspiral higher order modes, in particular observed quantities and measurement procedures. In the following, all quantities are referred to the whitened data as provided by the cWB pipeline. On-source data is meant to indicate the data at the gravitational wave event time; off-source data indicates data that do not include gravitational wave detections and provide independent noise instances of the data.

A signal is reconstructed by cWB as the estimated coherent response of the gravitational wave observatory, separated from the incoherent contributions of each detector, by means of the maximization of a constrained likelihood [2]. The cWB reconstruction provides a point estimate of the waveform. The expected statistical distribution of this estimate is built by repeating the same analysis on software injections of some signal model performed in off-source data. While each cWB analysis is a waveform-agnostic measurement of the signal content in the data, the signal model provides the reference hypothesis needed for the check of consistency. As a consequence, this procedure takes into account the actual noise characteristics of the observatory and the results are statistically conditioned to the correctness of the adopted signal model. To ensure an unbiased result, the key aspect of this procedure is the symmetry between the on-source and off-source analyses, in particular it is required that the settings of the cWB analysis be the same for on-source and off-source measurements. Signals similar to GW190814 are detected with efficiency very close to one and the cWB settings for investigating the waveform are the standard ones used for compact binary coalescence detection [14].

[1] An open source release of cWB is available at `https://gitlab.com/gwburst/public/library` with related documentation at `https://gwburst.gitlab.io/`.

The time-frequency representation of a signal is computed by the Wilson-Daubechies-Meyer (WDM) wavelet transform implemented in cWB [3]. In the following, time-frequency representations refers to the reconstructed signals at each detector, LIGO-Hanford, LIGO-Livingston and Virgo.

The waveform comparison is implemented by measuring the *waveform residual energy*, E_{res}, the sum of squared differences between the waveforms reconstructed by cWB, $W_k^{cWB}(t)$, and a waveform model, $W_k^{model}(t)$, taken as reference, where k indicates the detector and t is time. More specifically, E_{res} is computed in the time-frequency representation of the signal:

$$E_{res} = \sum_{k=1,2,3}^{det} \sum_{i=1,N}^{pixels} (w_k^{cWB}[i] - w_k^{model}[i])^2 \tag{1}$$

where $w[i]$ are the WDM trasforms of the $W(t)$ and the index i runs over all the WDM pixels which are part of the cWB reconstruction. [2] Alternative choices of test statistic are possible, but measuring the waveform residual energy naturally focuses on any discrepancies between the waveform-agnostic reconstruction and the signal model. Moreover, E_{res} proves to be more powerful than e.g. the match in some simulated quests for weak deviations from the signal model [5].

For a compact binary coalescence event, the signal model is provided by the set of waveform posteriors samples from a parameter estimation procedure based on Bayesian inference under the assumption of Gaussian noise [6, 7]. Assuming the correctness of a specific signal model, the reference distribution of the waveform residual energy E_{res} can be empirically assessed from a simulation, i.e. by running the cWB search on software signal injections performed in off-source data at different times. The use of off-source data at different times is necessary to assess the effect of actual noise fluctuations without making assumptions on the noise statistics. In each off-source experiment, a natural choice to compute E_{res} is to use the injected waveform posterior sample as reference W_k^{model}. The injections are randomly drawn from the set of waveform posterior samples and therefore the resulting off-source distribution of E_{res} takes into account also the uncertainties coming from the signal model. This empirical statistical distribution allows to set frequentist confidence intervals on the on-source measurement, assuming the correctness of the signal model. In particular, the $p-value$ of the on-source E_{res} can be used to test the consistency of the on-source cWB reconstruction with the signal model.

For the on-source measurement of E_{res}, the reference w_k^{model} in Eq.(1) is chosen to be the waveform posterior sample from the parameter estimation procedure which has the maximum likelihood value. Alternative choices are possible among the set of the waveform posterior samples, as e.g. the sample which has the maximum a posteriori probability or even a randomly selected sample. We selected the maximum likelihood sample since it minimizes the squared residuals with respect to the data in the Bayesian inference, and in this sense it is more data-oriented and more homogeneous to the cWB measurement of the waveform. Both the on-source cWB reconstruction and the bayesian inference are function of the same data and therefore the same input noise affects both reconstructions. Therefore, one can expect some positive correlation between the methods in terms of the statistical fluctuations of each on-source waveform with respect to its expectation value. Such a positive correlation may cause the on-source E_{res} to be underestimated with respect to the expectation value of the off-source estimates, where the "true" injected waveform is taken as reference.[3] This fact may add a bit of conservativeness to our tests of consistency between on-source and off-source E_{res}. In any case, the presence of this systematic effect can be checked by monitoring the distribution of on-source E_{res} resulting from taking as signal reference w_k^{model} in Eq. (1) many random draws of the posterior samples from the signal model.

[2] for more details see Sec. III.A of [5].

[3] A more symmetric procedure would be to repeat the Baysian inference estimate per each off-source signal injection and take as reference the maximum likelihood posterior sample. However, this is too computationally demanding to become feasible at the level of thousands of repetitions.

This kind of bias on the on-ource waveform energy residuals is however not expected in the case of the detection of subdominant modes, object of this note. In fact, as explained in the followig Section, the evaluation of E_{res} is restricted to a portion of the time-frequency representation inside which the considered signal model is null, and therefore insensitive by construction to the noise content of the data pertaining to that time-frequency volume.

In our current experience, we find that the off-source reference distribution is dominated by the composite effects of non Gaussian noise fluctuations of the data and of measurement uncertainty in the cWB reconstruction. The second contribution in order of relevance comes from the variability of waveform posteriors from the signal model. The variability of the power spectral density of the data, hence of the whitening filter used at different times, does not significantly affect the results.

3 Determination of the suitable time-frequency portion sensitive to inspiral higher order modes

The test of waveform consistency can be carried out over the full time-frequency volume of the candidate, as detected by cWB. Under this condition, the result is potentially sensitive to the largest variety of possible discrepancies between the reference model for the signal and its morphologically–agnostic reconstruction. However, by inspecting the full detected waveform, the test will be affected by the whole noise uncertainties, which may dilute the significance of any discrepancies. In case the scientific target is more specific, one can take advantage of the available prior information to focus the test within a smaller time-frequency volume, which can be tailored to be the most sensitive to the target, while at the same time least affected by the noise. This Section describes suitable time-frequency volumes for searching overtones and undertones of the dominant chirp emission during the inspiral of compact binary coalescences. In particular, it discusses the procedure to optimize the tailoring of such time-frequency regions.

A natural descpription of effects from possible subdominant modes, overtones and undertones, can be made in terms of frequency tracks centered at $\alpha \times f_{22}(t)$, where $f_{22}(t)$ is the prediction for the instantaneous frequency corresponding to the dominant mode, $(l = 2, m = 2)$, and α is a dimensionless real parameter [12, 13]. Subdominant modes at m are predicted to have a time-frequency track corresponding to $\alpha \simeq m/2$; however, this analysis will also search for frequency tracks not corresponding to standard integer m values.[4] A suitable a priori parametrization of the relevant *time-frequency slice* can then be as follows, see Fig. 1:

- include an evolving frequency band defined as $[\alpha - \delta\alpha, \alpha + \delta\alpha] \times f_{22}(t)$ Hz. This is centered on a given α–track and shows a fixed relative half width $\delta\alpha$, which is motivated both to provide a tolerance with respect to the modeled frequency evolution of subdominant modes and to take care of the finite resolution of the cWB time-frequency representation.

- limit the analyzed time range within $[t_{merger} - \Delta t, t_{merger} - \delta t]$ s. Δt is motivated by the robust expectation that subdominant modes may provide their strongest effects in the late inspiral phase only; δt is instead necessary to excise effects related to the merger phase which would leak into the inspiral time range because of the finite resolution of cWB.

- since all predictions agree that the $m = 3$ subdominant mode generates the strongest effect, it is wise to test separately the detection significance of the measurement at $\alpha = 1.5$.

- scan over an α range able to cover expected and unexpected contributions from subdominant modes, e.g. over grid values $0.5 - \delta\alpha < \alpha < 3 + \delta\alpha$, with step $\leq \delta\alpha$. This will result in multiple measure-

[4] Such subdominant modes are expected in General Relativity e.g. for the case of non circular orbits.

ments, correlated by the partial overlap of the time frequency slices. The final results as a function of α will need to be interpreted taking into account an effective trials factor.

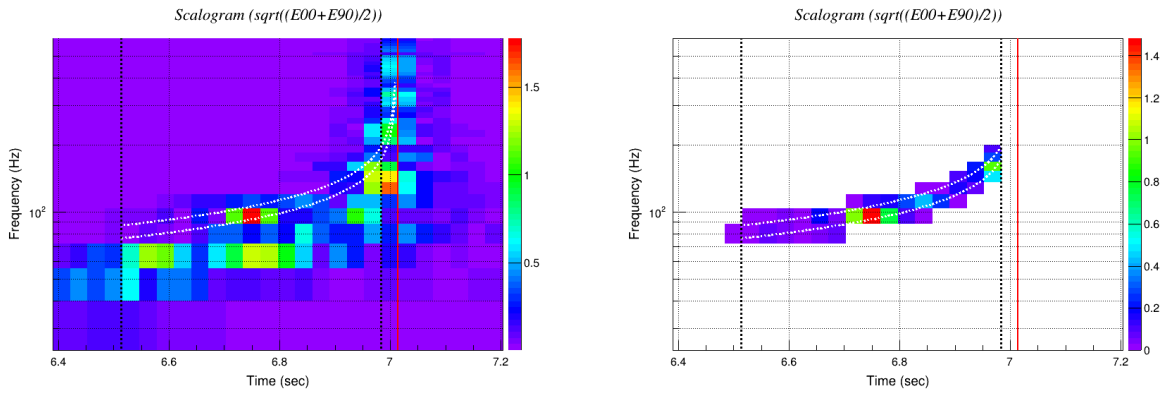

Figure 1: Time-frequency representation of the waveform residual energy of GW190814 in whitened data as measured by cWB, projected into the LIGO Livingston detector using the WDM transform with resolution $dt = 1/32$ s and $df = 16$ Hz. Left: time-frequency representation of the waveform residual energy of GW190814, used to evaluate E_{res}. Right: same but selecting the only time-frequency pixels which are included or partially overlapped with the time-frequency slice which is relevant for the detection of the $m = 3$ subdominant mode. These selection of pixels is used for the evaluation of $E_{res:TF}$. The red vertical line shows the merger time from the maximum likelihood `SEOBNRv4_ROM` waveform posterior. The dotted black vertical lines show the selected time range of the time-frequency slice, $[t_{merger} - 0.5$ s$, t_{merger} - 0.03$ s$]$. The white dotted curves delimit the selected frequency band of the time-frequency slice, here $[\alpha - 0.1, \alpha + 0.1] \times f_{22}(t)$ Hz with $\alpha = 1.5$.

The final waveform residual energy, $E_{res:TF}$ is built as defined by equation (1), with the restriction of summing over the only WDM pixels which pertain to the above described time-frequency slice. For the pixels which are partially included, their contributions to the waveform energy residual are weighted proportionally to the fraction of the pixel area occurring inside the time-frequency slice. This mitigates effects related to the finite time-frequency resolution of the WDM representation, and adds some correlation in the results from disjoint but adjacent time-frequency slices.

The optimization of the adopted time-frequency resolution of the WDM representation and of the shape of the time-frequency slice has been carried out by performing simulations of the measurement for the case $\alpha = 1.5$, i.e. detection of the $m = 3$ multipole, using data around the event time (off-source data). The optimization is based on measurements of the Receiver Operating Characteristic (ROC) [8], with the goal to select the setting which ensures the best balance between the rates of true positives (detection efficiency) vs false positives (false alarm probability) as a function of the test statistic $E_{res:TF}$. Montecarlo simulations in off-source data are implemented by injecting waveform posterior samples randomly drawn from the sets produced by Bayesian inference. [5] The measurements therefore include uncertainties from the model and from the actual noise statistics of the data and of the cWB reconstruction.

Aligned-spin Effective One Body waveform models without higher modes (`SEOBNRv4_ROM`, *null model*) and with higher modes (`SEOBNRv4HM_ROM`) [15] have been used to measure respectively the false alarm probability and the detection efficiency as a function of the measured waveform residual energy in the time-frequency slice, $E_{res:TF}$. The false alarm probability at $E_{res:TF}$ is computed as the fraction of off-source injections from the null model (`SEOBNRv4_ROM`) that are detected with a waveform residual energy greater

[5] the posterior samples are publicly available as supplementary material of [4].

or equal to $E_{res:TF}$. The evaluation of $E_{res:TF}$ is performed by using the injected waveform as reference w_k^{model}. The detection efficiency at $E_{res:TF}$ is instead computed as the fraction of off-source injections from the alternative model (`SEOBNRv4HM_ROM`) that are detected with a waveform residual energy greater or equal to $E_{res:TF}$. In this case, each waveform residual energy is evaluated from the cWB reconstruction of the injected waveform posterior from the `SEOBNRv4HM_ROM` model, but taking as reference the waveform obtained by switching off the higher order mode emission of the injected signal.

Figure 2 shows the ROC using a few variants of the tested settings defining the time-frequency slice, i.e. the parameters df, frequency resolution of the WDM representation, $\delta\alpha$, Δt. Each simulation consists in thousands of injections. The Receiver Operating Characteristic resulted weakly dependent on variations of the settings around our initial guess for the operating point ($df = 16$ Hz, $\delta\alpha = 0.15$, $\Delta t = 0.5$ s). Tested settings included $df = 8, 16, 32$ Hz, $\delta\alpha$ from 0.05 to 0.4, Δt from 0.2 to 0.6 s. The final choice of the time-frequency portion from the ROC optimization is $df = 16$ Hz, $\delta\alpha = 0.1$, $\Delta t = 0.5$ s. The choice of $\delta t = 0.03$ s has instead been driven to match the time duration of one pixel, in order to avoid to include significant contributions from the merger time, while at the same time it preserves the optimal ROC.

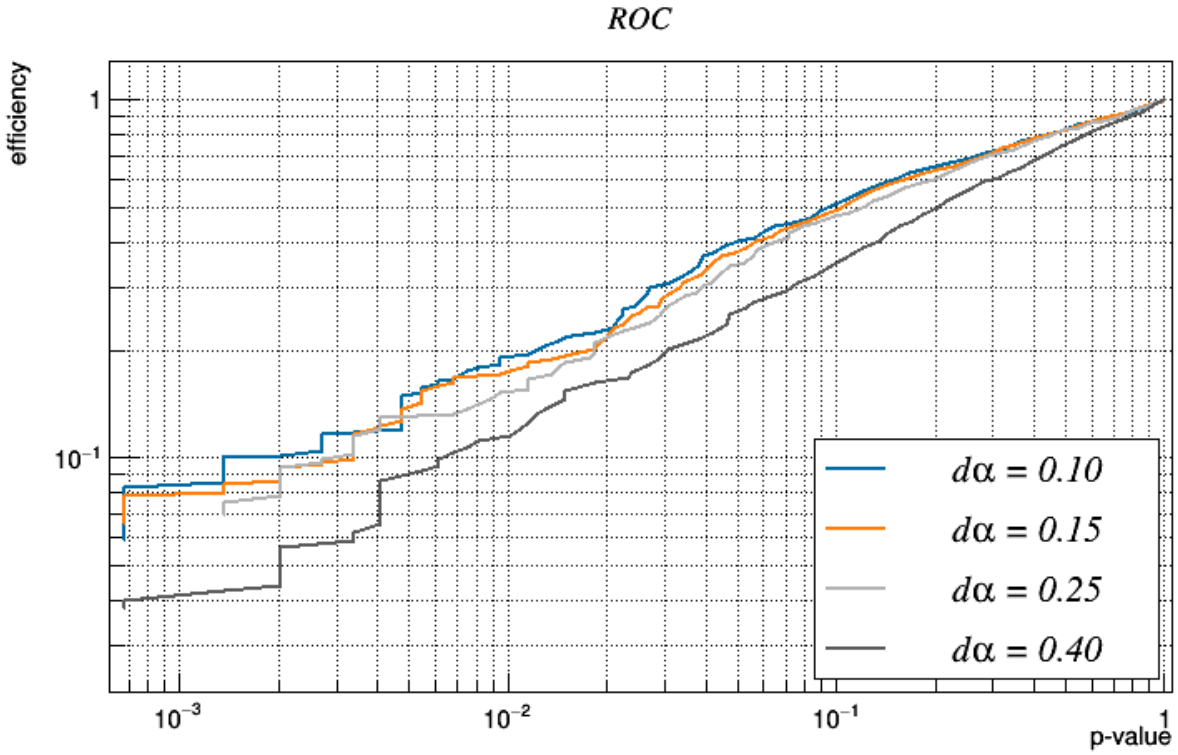

Figure 2: Samples of Receiver Operating Characteristic (ordinate: detection efficiency, abscissa: false alarm probability) for different choices of the $\delta\alpha$ parameter, with $df = 16$ Hz and $\Delta t = 0.5$ s. The optimal settings correspond to the upper curve.

Some figures of merit of this experiment can be easily extracted from the ROC: the cWB detection of the $m = 3$ mode in GW190814, according to the predictions of the `SEOBNRv4HM_ROM` waveform model, is expected to give a false alarm probability less than 1% (5%) for about 18% (40%) of the times. This means that this experiment has an interesting probability of detecting the $m = 3$ mode and as such it is sensitive enough to be pursued. Since the optimization of the time-frequency slice has been carried out usign only off-source data and with simulated signals, it does not pose any condition to the significance of the on-source results, e.g. no trial factors will be required by this optimization.

4 Performances of the method

The results related to GW190814 are presented in [4]. Here we give a deeper look to their interpretation and discuss some relevant checks that have been performed. We first discuss the measurement of the $m = 3$ subdominant mode and then the results for the wide range of tested time-frequency slices.

Figure 3 shows the GW190814 on-source result for $E_{res:TF}$ over its off-source distributions in the case of the time-frequency slice centered at $\alpha = 1.5$. It is evident that the on-source result is an outlier of the null model, `SEOBNRv4_ROM`, with a $p-value = 0.0068$. On the contrary, the on-source $E_{res:TF}$ is compatible to a random draw from the signal model including higher order modes, `SEOBNRv4HM_ROM`.

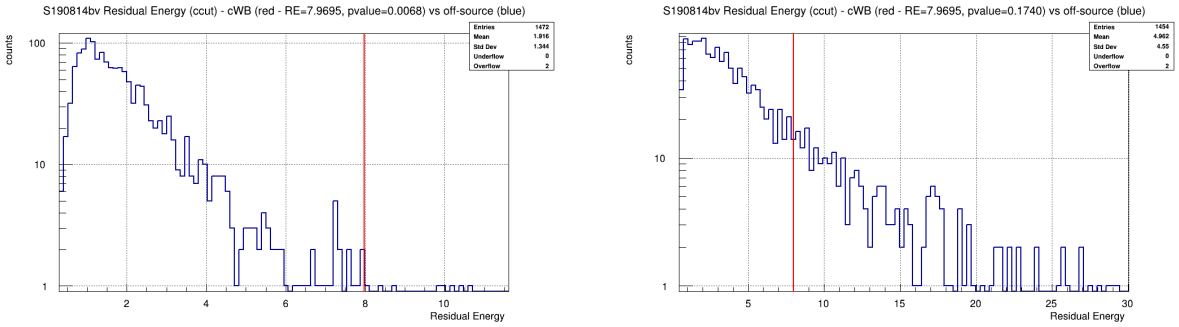

Figure 3: Waveform residual energy for the time-frequency slice centered at $\alpha = 1.5$. Red vertical line: on-source result for GW190814. Left: reference distribution of the null model from `SEOBNRv4_ROM` injections in off-source data. Right: reference distribution for the model with higher order modes, from `SEOBNRv4HM_ROM` injections in off-source data. The GW190814 result is an outlier of the null model and instead is compatible with the alternative model.

The same measurement has been repeated scanning the central α values from 0.4 to 3.3 in steps of 0.05. The ROC corresponding to the detection of the $m = 1, 4, 5$ modes are compared in Figure 4 with the ROC of the $m = 3$ detection: the performances of this method for the former set of modes are far from what is achieved for the latter (assuming that nature obeys to the `SEOBNRv4HM_ROM` signal model). It is also evident that in the case of $m = 1, 5$ modes of GW190814, this method is not performing significantly better than a blind random choice, which would be represented by a bisector of the quadrant. However, the motivation to scan over a wide range of α values using a waveform agnostic search is still valid, to exclude that unexpected energy be emitted in subdominant modes, in excess to the `SEOBNRv4HM_ROM` signal model.

Reference [4] reports the $E_{res:TF}$ $p-value$ vs α plot for the null hypothesis, represented by the `SEOBNRv4_ROM` signal model. There are no significant discrepancies with respect to the null model apart from the $m = 3$ mode, which means that we could not reject the `SEOBNRv4_ROM` predictions for $\alpha \neq 1.5$. In particular, cWB detects waveform energy residuals consistent with noise for $\alpha \sim 1$, which implies that the measured dominant $m = 2$ mode is consistent with the `SEOBNRv4_ROM` signal model.

The expections on the shape of the $p-value$ dip for $E_{res:TF}$ around $\alpha = 1.5$ has been investigated by looking at samples of the $p-value$ curves obtained from the detection efficiency simulations. Fig. 5 shows three such samples, which have been randomly selected imposing the condition $p-value < 0.01$ for $\alpha = 1.5$. These $p-value$ curves are representative of the most interesting fraction (18%) of the full set of results from the injections in off-source data of waveform posteriors from the `SEOBNRv4HM_ROM` signal model. Both the position of the $p-value$ minimum and the width of the dip vary according to the different noise features encountered by cWB. We conclude that the GW190814 result for the $p-value$ of $E_{res:TF}$ around $\alpha = 1.5$ is compatible with the simulated results. Results from further simulations, e.g. by injecting the same waveform posterior either from `SEOBNRv4HM_ROM` or `SEOBNRv4_ROM` signal models

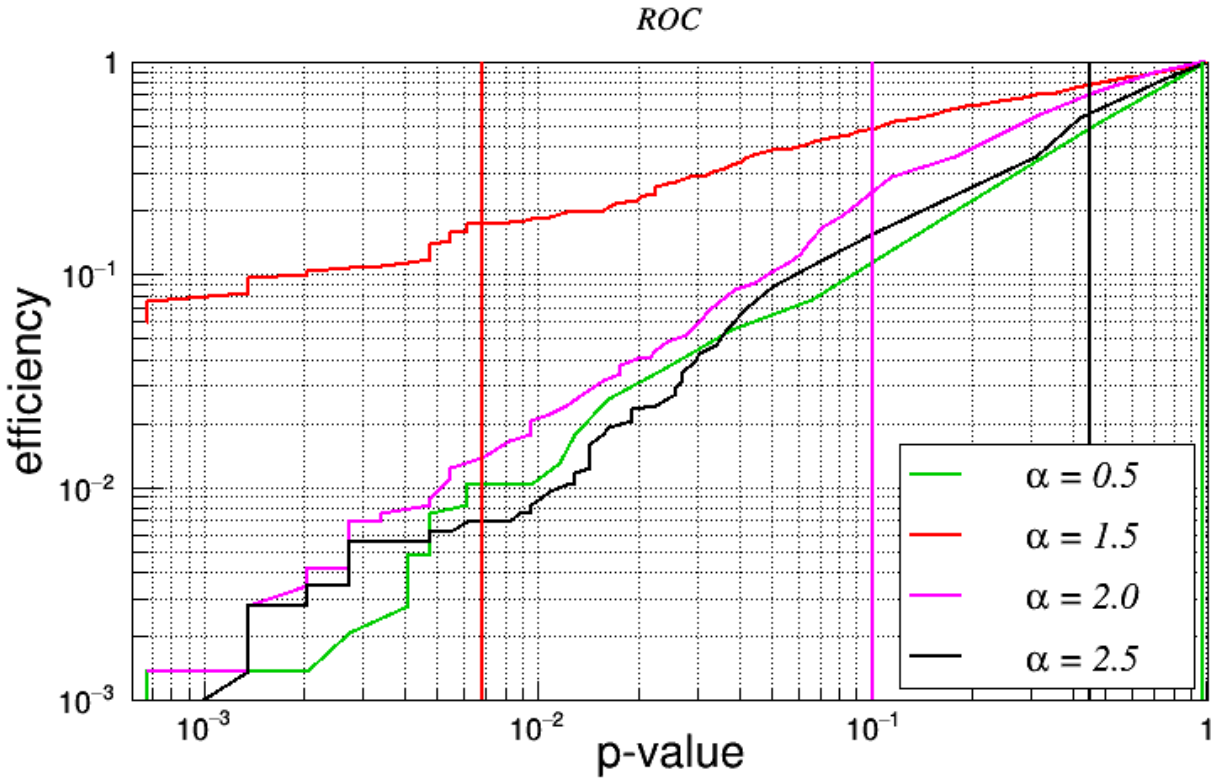

Figure 4: Comparison of Receiver Operating Characteristic for the detection of $m = 1, 3, 4, 5$ modes (green, red, magenta and black curves respectively). The ROCs assume a signal model given by the SEOBNRv4HM_ROM set of waveform posteriors. The performance of this experiment in the case of $m = 3$ is by far better than the performances for the other modes. In particular for $m = 1, 5$ the ROC are quite close to a blind random choice, which means that the experiment would be informative only in the case of unexpected excess energy in the $m = 1, 5$ modes. Vertical lines show the on-source $p - values$ with the same color code.

at different off-source times, show that the dominant source of fluctuations comes from the composite effect of non Gaussian noise in the data and of cWB reconstruction uncertainties.

To investigate the expected $p - value$ vs α curves in case inspiral higher order modes were absent in the signal, a few additional injections were performed off-source within 30 s of the GW190814 time from the SEOBNRv4_ROM model, see Figure 6. The frequent appearance of weak dips of $p - value$ is driven by the effective trials factor due to the scan along α. An upper limit to the trials factor is set by the number of disjoint time-frequency slices needed to cover the scanned α range, fifteen. However, the resulting trial factor will be lower due to the correlation in $E_{res:TF}$ coming from WDM pixels overlapping across adjacent slices. The $p - value$ curves in Fig. 6 are consistent with an effective trials factor $n \sim 10$: in fact, the plot shows that 2 out of 3 of the simulated $p - value$ vs α curves show a dip below 10%, which is comparable to the estimated probability of $1 - 0.90^n \sim 2/3$ ($1 - 0.95^n \sim 0.4$) that an injection from the SEOBNRv4_ROM signal model may show any $p - value$ dip below 10% (5%).

5 Conclusions and final remarks

This method for the detection of inspiral higher order modes in the gravitational wave emission from compact binary coalescences has been exploited in the discovery paper on GW190814 [4]. It is based on the

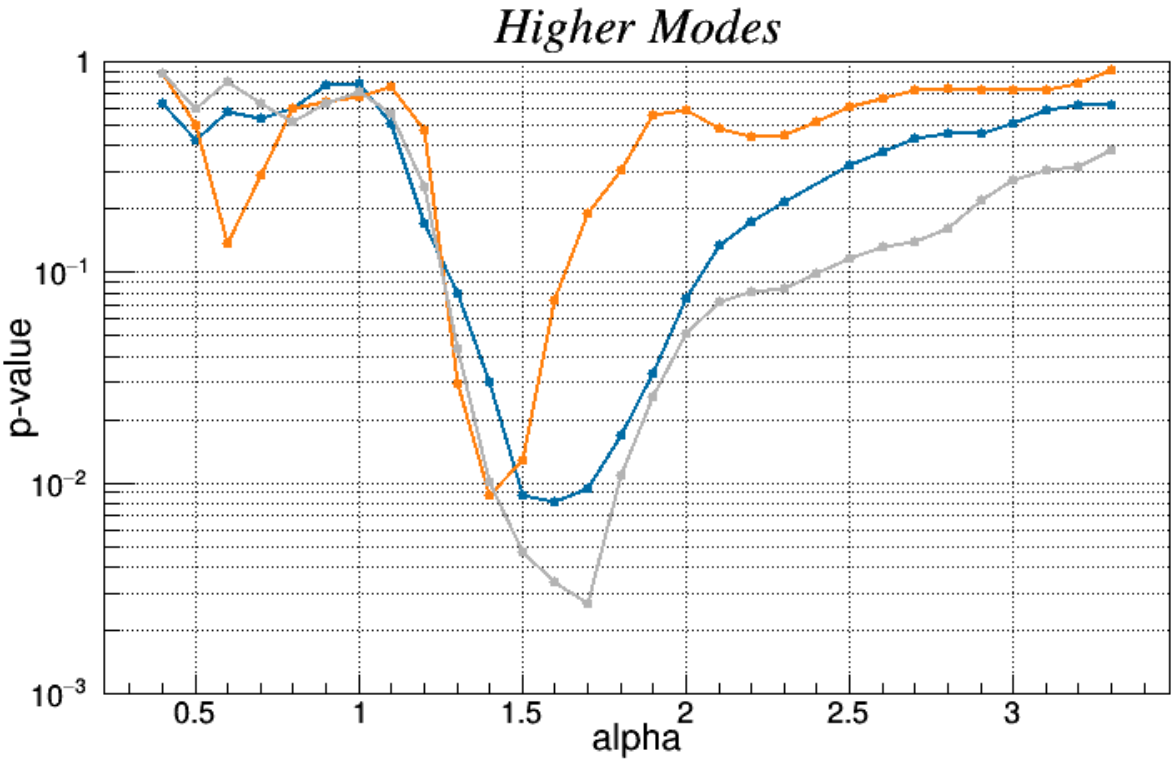

Figure 5: Simulated p-value curves selected from the off-source injections of waveform posteriors from the SEOBNRv4HM_ROM signal model. The selection is made under the requirement $p - value < 0.01$ for $\alpha = 1.5$ (they represent 18% of the full set). These cases give a sense of the expected variety of the $p-value$ dip around $\alpha = 1.5$.

coherentWaveBurst data analysis [2, 11], which provide waveform-agnostic detection and reconstruction of transient gravitational waves. In the case of GW190814, a null emission in the $m = 3$ multipole is rejected with a measured $p - value = 0.68\%$. Apart from the detection of the $m = 3$ mode, there are no other significant discrepancies with respect to the ($l = 2$,$m = 2$) model in a wide range of possible undertones and overtones of the dominant quadrupolar emission, parametrized with frequency tracks whose central frequency spans from 0.4 to 3.3 times the main quadrupolar emission. This method stems from our previous work [5] and implements a new procedure to include robust a priori information on the specific feature of the gravitational wave transient searched for. This is accomplished by focusing the coherent analysis of the data of the network of gravitational wave detectors to a specific portion of the time-frequency representation of the signal, selected by optimizing the Receiver Operating Characteristic. It provides a complementary procedure with respect to the time-frequency tracks method described by [12], whose results has been included in the GW190412 and GW190814 discovery papers [4, 13]. In fact, the latter analysis was performed using single detector data and makes a Gaussian noise assumption, even though it exploits an off-source calibration of the noise variance.

The main underlying idea is to test the consistency between the waveform measurements performed by coherentWaveBurst, which is making minimal assumptions on the gravitational wave transient, and the parametric estimates based on detailed waveform models, as provided by Bayesian inference. One peculiar capability of this method is to provide the composite uncertainty coming from the data and from the two different waveform measurements, thus enabling a direct measurement of consistency. This is accomplished by simulating of thousands of off-source repetitions of the experiment. The final results can be expressend

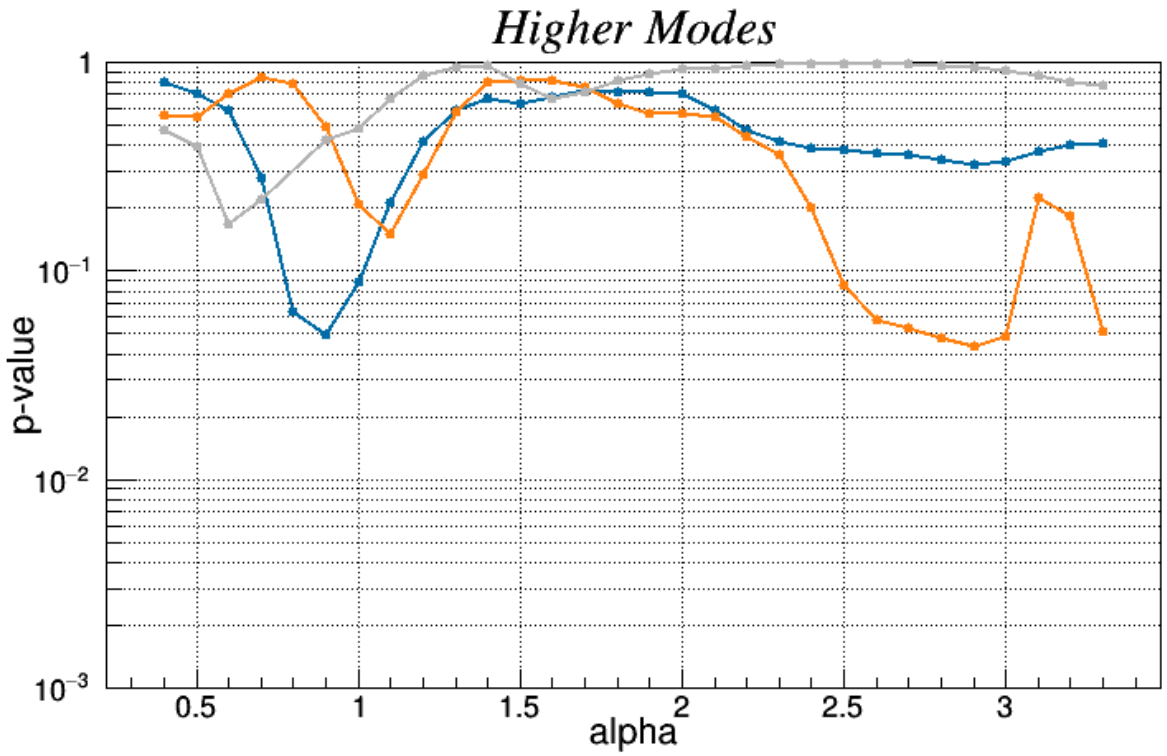

Figure 6: Simulated $p-value$ curves from three additional off-source injections of waveform posteriors from the null signal model, `SEOBNRv_ROM`, performed within 30s of GW190814. The presence of weak dips in the $p-value$ is consistent with an effective trials factor of order 10.

as frequentist $p-values$ or confidence intervals for the on-source measurement, assuming the correctness of the signal model. In particular, the method does not make any assumption on the noise statistics of the data and, in fact, our current experience shows that the dominant source of statistical fluctuations comes from the composite effect of non Gaussian noise in the detectors' data with the uncertainties in the coherentWaveBurst reconstruction.

These procedures can be extended to analyse other different features of gravitational wave transients whose time-frequency representation is understood a priori and therefore a time-frequency region can be tailored to the scope. Applications can include the investigation of features in the spectra or in the luminosity profiles, of post-merger emissions, precursors, memory effects. Work is in progress to develop more of these capabilities and test them on actual observations.

Acknowledgements

The authors are grateful for computational resources provided by the LIGO Laboratory and supported by National Science Foundation Grants PHY-0757058 and PHY-0823459. ST is supported by University of Zurich Forschungskredit Nr. FK-19-114 and Swiss National Science Foundation.

References

[1] B. P. Abbott, R. Abbott, T. D. Abbott, S. Abraham, F. Acernese, K. Ackley, C. Adams, V. B. Adya, C. Affeldt, M. Agathos, et al., A guide to ligo–virgo detector noise and extraction of transient gravitational-wave signals, Classical and Quantum Gravity 37 (5) (2020) 055002. doi:10.1088/1361-6382/ab685e.
URL http://dx.doi.org/10.1088/1361-6382/ab685e

[2] S. Klimenko, G. Vedovato, M. Drago, F. Salemi, V. Tiwari, G. Prodi, C. Lazzaro, K. Ackley, S. Tiwari, C. Da Silva, et al., Method for detection and reconstruction of gravitational wave transients with networks of advanced detectors, Physical Review D 93 (4). doi:10.1103/physrevd.93.042004.
URL http://dx.doi.org/10.1103/PhysRevD.93.042004

[3] V. Necula, S. Klimenko, G. Mitselmakher, Transient analysis with fast Wilson-Daubechies time-frequency transform, J. Phys. Conf. Ser. 363 (2012) 012032. doi:10.1088/1742-6596/363/1/012032.

[4] LIGO Scientific Collaboration and Virgo Collaboration, GW190814: Gravitational waves from the coalescence of a 23 solar mass black hole with a 2.6 solar mass compact object, The Astrophysical Journal 896 (2) (2020) L44. doi:10.3847/2041-8213/ab960f.
URL https://doi.org/10.3847%2F2041-8213%2Fab960f

[5] F. Salemi, E. Milotti, G. A. Prodi, G. Vedovato, C. Lazzaro, S. Tiwari, S. Vinciguerra, M. Drago, S. Klimenko, Wider look at the gravitational-wave transients from gwtc-1 using an unmodeled reconstruction method, Phys. Rev. D 100 (2019) 042003. doi:10.1103/PhysRevD.100.042003.
URL https://link.aps.org/doi/10.1103/PhysRevD.100.042003

[6] J. Veitch, V. Raymond, B. Farr, W. Farr, P. Graff, S. Vitale, B. Aylott, K. Blackburn, N. Christensen, M. Coughlin, et al., Parameter estimation for compact binaries with ground-based gravitational-wave observations using the lalinference software library, Physical Review D 91 (4). doi:10.1103/physrevd.91.042003.
URL http://dx.doi.org/10.1103/PhysRevD.91.042003

[7] G. Ashton, M. Hübner, P. D. Lasky, C. Talbot, K. Ackley, S. Biscoveanu, Q. Chu, A. Divakarla, P. J. Easter, B. Goncharov, et al., Bilby: A user-friendly bayesian inference library for gravitational-wave astronomy, The Astrophysical Journal Supplement Series 241 (2) (2019) 27. doi:10.3847/1538-4365/ab06fc.
URL http://dx.doi.org/10.3847/1538-4365/ab06fc

[8] T. Fawcett, An introduction to roc analysis, Pattern Recognition Letters 27 (8) (2006) 861 – 874, rOC Analysis in Pattern Recognition. doi:https://doi.org/10.1016/j.patrec.2005.10.010.
URL http://www.sciencedirect.com/science/article/pii/S016786550500303X

[9] S. Klimenko, G. Mitselmakher, A wavelet method for detection of gravitational wave bursts, Class. Quant. Grav. 21 (2004) S1819–S1830. doi:10.1088/0264-9381/21/20/025.

[10] S. Klimenko, S. Mohanty, M. Rakhmanov, G. Mitselmakher, Constraint likelihood analysis for a network of gravitational wave detectors, Phys. Rev. D 72 (2005) 122002. arXiv:gr-qc/0508068, doi:10.1103/PhysRevD.72.122002.

[11] M. Drago, V. Gayathri, S. Klimenko, C. Lazzaro, E. Milotti, G. Mitselmakher, V. Necula, B. O'Brian, G. A. Prodi, F. Salemi, M. Szczepanczyk, S. Tiwari, V. Tiwari, G. Vedovato, I. Yakushin, Coherent [waveburst], a pipeline for unmodeled gravitational-wave data analysis (2020). arXiv:2006.12604.

[12] S. Roy, A. S. Sengupta, K. G. Arun, Unveiling the spectrum of inspiralling binary black holes (2019). arXiv:1910.04565.

[13] LIGO Scientific Collaboration and Virgo Collaboration, GW190412: Observation of a binary-black-hole coalescence with asymmetric masses (2020). arXiv:2004.08342.

[14] B. P. Abbott, et al., GWTC-1: A Gravitational-Wave Transient Catalog of Compact Binary Mergers Observed by LIGO and Virgo during the First and Second Observing Runs, Phys. Rev. X 9 (3) (2019) 031040. arXiv:1811.12907, doi:10.1103/PhysRevX.9.031040.

[15] R. Cotesta, A. Buonanno, A. Bohé, A. Taracchini, I. Hinder, S. Ossokine, Enriching the symphony of gravitational waves from binary black holes by tuning higher harmonics, Phys. Rev. D 98 (2018) 084028. doi:10.1103/PhysRevD.98.084028.
URL https://link.aps.org/doi/10.1103/PhysRevD.98.084028